Applied Environmental Research
- RESEARCH FOR SUSTAINABLE PLANET -

Research Article

Spatial Estimation of Trophic State for Reservoir Using Ground Monitoring and Remote Sensing Data

Thong Nguyen Hoang[1,2], Van Tran Thi[1,2,*]

[1] *Faculty of Environment and Natural Resources, Ho Chi Minh City University of Technology (HCMUT), Ho Chi Minh City, Vietnam*
[2] *Vietnam National University Ho Chi Minh City, Ho Chi Minh City, Vietnam*

*Corresponding Email: tranthivankt@hcmut.edu.vn

Abstract

Nutrient pollution, also known as eutrophication, is a severe environmental problem that leads to harmful algal blooms in water bodies and affects water supplies for human use. This study aims to determine the trophic state of the reservoir based on the trophic state index (TSI) calculated from ground monitoring data of Secchi depth (SD), total phosphorus (TP), and chlorophyll-a (Chl-a) obtained from 35 points in 2 survey periods during the late rainy season to early dry season 2012–2013 and May 2023. In addition, we combined remote sensing data to spatially estimate the eutrophication situation across the reservoir through correlation analysis and determine the best regression models. The results of correlation analysis between ground monitoring values and spectral values from remote sensing algorithms showed that the two parameters, SD and TP, correlated best with the NIR/BLUE algorithm. In contrast, the Chl-a parameter correlated best with the NIR/RED algorithm. From there, we mapped the spatial distribution of parameters and trophic state according to TSI in the entire Dau Tieng Reservoir based on the spectral values from remote sensing algorithms and regression models. Analysis results showed that, as of May 2023, the Dau Tieng Reservoir showed signs of eutrophication in most areas; some areas also showed signs of hyper-eutrophication, causing the risk of harmful algal blooms. The results achieved in this study will be a valuable source of consultation, supporting environmental management to minimize nutrient pollution in the Dau Tieng Reservoir water source.

ARTICLE HISTORY

Received: 13 Sep. 2024
Accepted: 11 Dec. 2024
Published: 29 Jan. 2025

KEYWORDS

Eutrophication;
Nutrient pollution;
TSI;
Remote sensing;
Reservoir

Introduction

In recent decades, the world's population explosion has led to the rapid development of urban areas, combined with the trend of industrialization, increased production, and global economic growth, causing many negative impacts on the environment. One of the most significant impacts of industrialization and urbanization trends is the discharge of pollutants into the environment. Nutrient pollution, also known as eutrophication, occurs when water sources become overloaded with minerals and nutrients, particularly nitrogen and phosphorus [1]. In addition, this phenomenon is defined as an increase in the productivity of phytoplankton mediated by nutrients [2]. Nutrients from water sources promote the growth and development of phytoplankton species, mainly algae. One of the most frequent negative effects of nutrient pollution is algal blooms. They severely reduce the amount of dissolved oxygen in water, thereby causing aquatic organisms to suffocate due to a lack of oxygen [3]. Some algal species are also capable of generating toxins that can poison organisms and cause death [4]. The serious harmful effects caused by eutrophication have created an urgent need to monitor and supervise this phenomenon to provide quick and timely warnings. Nonetheless, monitoring eutrophication levels covering a large region via traditional measurement methods is difficult and costly. Furthermore, assessing the level of nutrient pollution depends on many water environment

https://doi.org/10.35762/AER.2025001

parameters. Therefore, monitoring via traditional methods on a large spatial scale over a long period requires much effort. Remote sensing methods have outstanding advantages in the spatial and temporal monitoring of large research areas on the basis of satellite image data. In combination with ground monitoring data, remote sensing methods can estimate the quantitative value of objects (such as area and concentration). This makes tracking and monitoring research subjects more accessible and convenient.

Globally, the application of remote sensing technology in assessing the nutritional status of water bodies on the basis of the TSI has only been widely applied in the last two decades. Some prominent studies can be mentioned as follows: In 2007, Duan et al. used the NIR/RED band ratio, which is commonly used in algal bloom monitoring studies [5–7], from Landsat-5 satellite imagery to construct a regression model to estimate the Chl-a concentration and evaluate the trophic state of Chagan Lake, China. The results indicate that the regression model can effectively determine the Chl-a concentration and evaluate the trophic state of a lake [8]. In 2014, Papoutsa et al. [9] studied four seas in the Mediterranean, Cyprus and Greece to find the best satellite image band ratio to estimate the SD value, one of three commonly used parameters to evaluate the trophic state. The results showed that the exponential regression model from the GREEN/RED band ratio best estimates the SD value. In 2016, Membrillo et al. [10] used the RED band and the NIR/RED band ratio of satellite imagery to estimate turbidity and Chl-a concentrations in the Chapala Reservoir, Mexico. The estimated turbidity and Chl-a values from the best linear regression models have errors of 11% and 27%, respectively. In 2019, Shi et al. [11] conducted a large-scale study in which remote sensing methods were used to estimate the trophic state of Qiandaohu Lake, China. The regression model in this study was built from 812 water monitoring samples collected from 27 lakes in China from 2004-2018. The results of the estimation of the TSI value at Qiandaohu Lake indicate a good correlation between the 440 nm wavelength absorption and the SD, total nitrogen (TN), total phosphorus (TP), and Chl-a parameters. In 2022, Lyu et al. [12] conducted another study to estimate the trophic state of seven lakes in Northeast China via remote sensing methods. The dataset used in the study included SD, TP, and Chl-a data from water samples collected in October 2010. They calculated the TSI value according to the formula proposed by Carlson in 1977. The TSI estimation results from the present study are relatively good, with a high level of correlation between ground monitoring data and reflectance values obtained from a handheld spectrometer and errors between the quantification results from remote sensing methods and ground monitoring data being relatively low [13].

In Vietnam, TSI has been applied in several studies to assess the trophic state of water bodies in recent years. In 2017, Nguyen et al. [14] used Landsat-8 satellite image data to evaluate the current trophic state of Linh Dam Lake, Hanoi, via remote sensing methods. The study proposed assessing the trophic state on the basis of the TSI value of Chl-a. The results of the study indicated that the BLUE/GREEN ratio band had the best correlation with the TSI value calculated from ground Chl-a data and could be used to estimate the TSI value for the entire lake area. Additionally, in 2017, studies by Tuan et al. at Blue Reservoir, Haiphong city, and Ngoc et al. at some urban lakes in Hanoi assessed the trophic state according to the TSI. Both of the above studies were conducted via a representative sampling method, with SD, TP, and Chl-a. Then, the TSI value was calculated via Carlson's proposed formula [15–16]. In 2020, Thuan et al. [17] presented an overview of the recent eutrophication situation in Hanoi lakes from previous studies and evaluated the case of Cu Chinh Lake. This study used the TSI calculated from the parameters TN, TP, and Chl-a as proposed by Carlson & Simpson in 1996 [18] to evaluate the eutrophication of the lake instead of the TSI proposed by Carlson in 1977 [12]. However, these studies are limited in their use of monitoring points to assess the trophic state of the lake. In 2021, Thao et al. conducted research on monitoring changes in the eutrophication of Hoan Kiem Lake on the basis of Chl-a concentrations calculated from Sentinel-2A satellite images collected from September 2019 to August 2020. The survey results from 50 monitoring points at Hoan Kiem Lake at 5 different times of the year show that the Chl-a concentration is highly correlated with the reflectance value of the NIR/RED band ratio. Research has indicated that this ratio band and exponential regression equation can be applied to calculate the Chl-a concentration in water bodies [19]. In general, studies using the TSI index to assess the trophic state of water bodies in Vietnam are carried out via two methods: (i) assessment on the basis of several representative monitoring points, which represents only the nutrient status at those points instead of assessing the entire research area; and (ii) assessment of the entire study area via remote sensing methods but is only based on the Chl-a parameter.

The research area is the Dau Tieng Reservoir, located upstream of the Saigon River, in the territory of three provinces: Tay Ninh, Binh Phuoc, and Binh Duong (Figure 1). The reservoir started construction in 1985 and is Vietnam's largest artificial irrigation reservoir. The Dau Tieng Reservoir plays a significant role in regulating flow, preventing floods, repelling salinity, and providing water for daily life and agricultural production in the region and downstream of the Saigon

River. In recent years, the water quality at Dau Tieng Reservoir has been declining and has shown signs of eutrophication due to impacts from sand mining activities, aquaculture, and agricultural cultivation in alluvial areas [20]. These activities contribute a large amount of nutrients to the water environment, causing eutrophication, and are among the leading causes of algae growth in reservoirs [21]. Therefore, to investigate the potential of remote sensing in monitoring and assessing nutrient pollution by integrating multiple parameters, we initiated this study to evaluate the feasibility of the technique. In the case of positive results, this study could lead to the application of remote sensing to assist management agencies in managing and protecting the water environment of Dau Tieng Reservoir and other reservoirs. This approach could offer practical benefits and result in significant cost and time savings compared with the current traditional water sample collection methods used in Vietnam.

Data and methods

1) Data collection

1.1) Ground monitoring data

The ground monitoring data included the SD (m), TP (mg L^{-1}), and Chl-a (µg L^{-1}) data (Table 1), which were collected in two phases. Phase 1 is the late rainy season to the early dry season from 2012–2013. Data on parameters during this period were collected at five monitoring points—October 22, 2012; November 27, 2012; December 22, 2012; January 26, 2013; and February 27, 2013—from the studies of Pham et al. [21] in 2017 and Thong et al. [20] in 2023. In phase 2, at the beginning of the rainy season in May 2023, data were collected at ten monitoring points on May 6, 2023. The locations of the monitoring points in both phases are shown in Figure 1.

The SD parameter is measured via a Secchi disk with a diameter of 20 cm, which is attached to a 3 m long wire with marked points, each 10 cm apart, to read the measurement results. The Secchi disk is slowly lowered into the water, and the first depth value is read when the disk is no longer visible. Then, it is lowered to another 0.5 m depth, lifted slowly, and the depth value is read a second time when the disc is visible. The average depth value of the two readings is the SD value. The samples analyzed for TP and Chl-a were collected 0.5 m below the water surface and stored refrigerated at 4°C. The TP concentrations were analyzed according to the Standard Methods for the Examination of Water and Wastewater (SMEWW) 4500-P of the American Public Health Association (APHA) through two steps: con-version of the phosphorus form of interest to dissolved orthophosphate and colorimetric determination of dissolved orthophosphate [22]. The Chl-a concentration was analyzed according to the SMEWW 10200-PLANKTON of APHA by measuring the absorbance of the phytoplankton extract in 90% acetone solution before and after standardization with the solution at wavelengths of 665 and 750 nm [23].

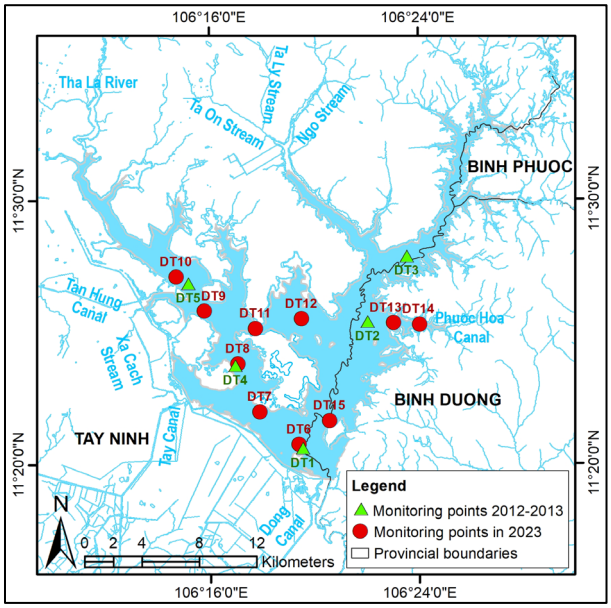

Figure 1 Study area and locations of ground monitoring points.

Table 1 Ground monitoring data of SD, TP, and Chl-a

Monitoring points	SD (m)	TP (mg L^{-1})	Chl-a (µg L^{-1})	Monitoring points	SD (m)	TP (mg L^{-1})	Chl-a (µg L^{-1})
DT1-Oct-2012	1	0.06	6.49	DT4-Jan-2013	1.5	0.06	4.15
DT2-Oct-2012	1	0.07	10.93	DT5-Jan-2013	1.1	0.06	2.96
DT3-Oct-2012	0.9	0.08	16.68	DT1-Feb-2013	1.8	0.05	0.46
DT4-Oct-2012	0.7	0.08	11.63	DT2-Feb-2013	1.5	0.05	2.53
DT5-Oct-2012	0.6	0.10	13.88	DT3-Feb-2013	1.4	0.06	5.94
DT1-Nov-2012	1.7	0.06	1.00	DT4-Feb-2013	1.7	0.05	4.24
DT2-Nov-2012	1.9	0.05	2.94	DT5-Feb-2013	1.3	0.05	5.23
DT3-Nov-2012	1.8	0.07	2.98	DT6-May-2023	0.7	0.08	7.67
DT4-Nov-2012	1.6	0.05	3.10	DT7-May-2023	0.8	0.06	7.32
DT5-Nov-2012	1.3	0.07	9.57	DT8-May-2023	0.6	0.07	8.24
DT1-Dec-2012	1.4	0.04	1.49	DT9-May-2023	0.4	0.08	9.15

Table 1 Ground monitoring data of SD, TP, and Chl-a (*continued*)

Monitoring points	SD (m)	TP (mg L^{-1})	Chl-a (µg L^{-1})	Monitoring points	SD (m)	TP (mg L^{-1})	Chl-a (µg L^{-1})
DT2-Dec-2012	1.4	0.05	4.75	DT10-May-2023	0.4	0.08	9.61
DT3-Dec-2012	1.1	0.06	8.98	DT11-May-2023	0.4	0.06	10.76
DT4-Dec-2012	1.5	0.04	2.44	DT12-May-2023	0.7	0.08	9.27
DT5-Dec-2012	1.3	0.05	4.60	DT13-May-2023	0.5	0.08	9.50
DT1-Jan-2013	2	0.04	2.84	DT14-May-2023	0.5	0.09	13.65
DT2-Jan-2013	1.4	0.05	1.31	DT15-May-2023	0.9	0.05	6.64
DT3-Jan-2013	1.4	0.05	1.61				

1.2) Satellite data

The satellite image data used in the study include Landsat-7 images acquired during the late rainy season to early dry season from 2012–2013 (October 22, 2012; November 27, 2012; December 22, 201; January 26, 2013; February 27, 2013) and Landsat-8 images acquired on May 6, 2023, with the same spatial resolution of 30 m space. The path/row of the satellite images is 125/052. The time at which satellite image data are collected coincides with the time at which field samples are collected for analyzing parameters.

2) Method to evaluate the trophic state

In this study, the trophic state of the Dau Tieng Reservoir was evaluated according to the TSI value calculated via Eq. 1. The TSI, proposed by Carlson in 1977, is a popular index used to assess the trophic status of water bodies. Carlson's TSI can be calculated on the basis of independent values of one of three parameters, namely, the SD value (m), TP concentration (mg L^{-1}), and Chl-a concentration (µg L^{-1}), according to Eqs. 2–4 or a combination of all three parameters according to Eq. 1 [12]. The trophic state of Dau Tieng Reservoir is classified into four levels, namely, oligo-trophic, meso-trophic, eutrophic, and hypertrophic, on the basis of the threshold values presented in Table 2.

$$\text{Carlson's TSI} = \frac{\text{TSI (SD)}+\text{TSI (TP)}+\text{TSI (Chl-a)}}{3} \quad \text{(Eq. 1)}$$

In which:

$$\text{TSI (SD)} = 60 - 14.41\ln(\text{SD}) \quad \text{(Eq. 2)}$$

$$\text{TSI (TP)} = 14.42\ln(1000\text{TP}) + 4.15 \quad \text{(Eq. 3)}$$

$$\text{TSI (Chl-a)} = 9.81\ln(\text{Chl-a}) + 30.6 \quad \text{(Eq. 4)}$$

3) Remote sensing methods

Remote sensing methods can identify and monitor objects or environmental conditions from a distance by analyzing their reflection and radiation with electromagnetic wavelengths without requiring direct contact. To extract and correctly identify information about objects, it is necessary to determine their spectral reflectance characteristics with electromagnetic wavelengths. The research objects of this study are nutritional parameters, including SD, TP, and Chl-a. Therefore, determining the spectral reflectance characteristics of these parameters is the foundation for choosing appropriate satellite image bands in remote sensing algorithms to monitor the trophic state. The spectral reflectance characteristics of Chl-a are most evident at wavelengths in the visible and near-infrared (NIR) spectra [24–25]. Chl-a absorbs most of the light radiation in the blue and red bands, with absorption peaks at wavelengths of approximately 433 and 686 nm, respectively [25]. In the green and NIR bands, Chl-a reflects most light radiation with reflection peaks at wavelengths of approximately 550 and 715 nm [24], creating the green color of Chl-a. This color is related to high light scattering and low light absorption in the green and near-infrared regions of phytoplankton cell walls [24, 26]. Unlike Chl-a, few studies have focused on the spectral reflectance characteristics of the TP. However, it is possible to use the spectral reflectance characteristics of colored dissolved organic matter (CDOM) in water, which is created from the decomposition of organic matter, to identify TP [27–28]. CDOM most strongly absorbs light with short wavelengths ranging from blue to ultraviolet, whereas pure water absorbs red light with longer wavelengths [29]. Therefore, water with a low CDOM concentration is blue, and vice versa. Both the CDOM and Chl-a components in water absorb light in the same blue spectral range, which can lead to errors in identifying these two components in aquatic environments [6, 29]. Consequently, the use of the blue band to quantify the Chl-a content in water is often ineffective [6]. For the SD parameter, many factors can affect the SD value, such as suspended sediments, phytoplankton, and CDOM. All of these factors can reduce light transmission in water, thereby reducing the SD value. Because many components affect the SD, it is difficult to determine specific spectral reflectance characteristics for this parameter. However, the identification of SDs can be based on the spectral reflectance characteristics of CDOM or Chl-a because these components directly affect SDs. Generally, the spectral characteristics of the three parameters SD, TP, and Chl-a are shown in the visible region and part

of the NIR spectral range. Therefore, the BLUE, GREEN, RED, and NIR bands of satellite images are used in the remote sensing algorithms for parameters. The remote sensing algorithms used in the study are presented in Table 3.

4) Statistical methods

4.1) Correlation analysis

Correlation analysis is a method of evaluating and measuring the correlation between two or more variables. This study uses correlation analysis to measure the correlation between two variables: spectral values extracted from remote sensing algorithms (x) and ground monitoring values (y). Many types of correlation coefficients are used in statistics and data analysis; however, in this study, we focus only on the Pearson correlation coefficient (R) to test the linear relationship between the independent and dependent variables. R is calculated according to Eq. 5. The value of R ranges from -1 to +1. The closer the absolute value of R is to 1, the greater the linear correlation between the variables. Twenty-five ground monitoring samples in phase 1 of each para-meter are used to analyze their correlation with the spectral values extracted from the remote sensing algorithms.

$$R = \frac{\sum(x_i - \bar{x})(y_i - \bar{y})}{\sqrt{\sum(x_i - \bar{x})^2 \sum(y_i - \bar{y})^2}} \quad \text{(Eq. 5)}$$

where $\bar{x}$ and $\bar{y}$ are the mean values of x and y, respectively.

To assess whether the correlation between two variables, x and y, is statistically significant or random, we use SPSS software to calculate the p value. The null hypothesis (H_0) is set up as follows: there is no statistical significance between the variables, there is no linear correlation, and the observed correlation is random. Suppose the p value is lower than the significance level (typically < 5%). In that case, there is enough evidence to reject H_0 and confirm that the linear relationship between the two variables is statistically significant. In contrast, a high p value indicates insufficient evidence to reject H_0, meaning that the relationship between the variables is not strong enough to be confirmed as statistically significant.

4.2) Regression model

The algorithms that best correlated with the ground monitoring values of each parameter based on R and had a p value < 5% were used to construct linear regression models to calculate the values of the parameters in the water based on the spectral values extracted from the remote sensing algorithms. To evaluate the appropriateness and rigour of the regression model, we used the coefficient of determination (R^2), which is calculated by the square of R. This index indicates the percentage of variation in the dependent variable that the model explains. The value of R^2 ranges from 0 to 1; the closer it is to 1, the more the regression model explains the entire variation in the dependent variable. In other words, the more rigorous and appropriate the regression model is.

4.3) Validation

The forecast values of the parameters calculated from regression models must be validated for accuracy. The accuracy assessment method used is forecast error, which is calculated as the difference between the actual value (ground monitoring) and the forecast value (regression model). A lower forecast error indicates that the model is more accurate in its predictions, whereas a higher forecast error indicates that the model may need to be adjusted or improved. The mean absolute error (MAE) (Eq. 6), mean absolute percentage error (MAPE) (Eq. 7), and root mean squared error (RMSE) (Eq. 8) are forecast errors used to evaluate the accuracy of the forecast values calculated from the regression model in this study.

Table 2 Relationships between SD, TP, Chl-a, and TSI values and trophic level [18]

TSI	SD (m)	TP (mg L^{-1})	Chl-a (µg L^{-1})	Trophic state
0–40	4–8	0–0.012	0–2.6	Oligotrophic
40–50	2–4	0.012–0.024	2.6–7.3	Mesotrophic
50–70	0.5–2	0.024–0.096	7.3–56	Eutrophic
> 70	< 0.5	> 0.096	> 56	Hypertrophic

Table 3 Remote sensing algorithms used in this study

Algorithm	Abbreviati	Equation	Reference
Blue band	BLUE	BLUE	
Green band	GREEN	GREEN	
Red band	RED	RED	
Near infrared band	NIR	NIR	

Table 3 Remote sensing algorithms used in this study (*continued*)

Algorithm	Abbreviatio	Equation	Reference
Band Ratio 1	BR1	GREEN/BLUE	
Band Ratio 2	BR2	RED/BLUE	
Band Ratio 3	BR3	NIR/BLUE	
Band Ratio 4	BR4	RED/GREEN	
Band Ratio 4	BR5	NIR/GREEN	
Ratio vegetation index	RVI	NIR/RED	[30]
Normalized difference vegetation index	NDVI	(NIR – RED)/(NIR + RED)	[31]
Normalized difference water index	NDWI	(GREEN – NIR)/(GREEN + NIR)	[32]
Normalized difference turbidity index	NDTI	(RED – GREEN)/(RED + GREEN)	[33]
Normalized difference suspended sediment index	NDSSI	(BLUE – NIR)/(BLUE + NIR)	[34]

Ten ground monitoring samples in phase 2 are used to assess the accuracy of the forecast values of the parameters from the regression model. If the forecast values calculated from the regression models meet the accuracy validation requirements, we use the regression models to map the spatial distributions of the SD, TP, and Chl-a parameters. These parameters are then applied to Eqs. 1–4 to calculate the TSI value and estimate and map the trophic state. The methodological diagram of the steps performed in the study is presented in Figure 2.

$$MAE = \frac{\sum_{i=1}^{n}|y_i - z_i|}{n} \quad \text{(Eq. 6)}$$

$$MAPE = \frac{\sum_{i=1}^{n}\frac{|y_i - z_i|}{y_i}}{n} \quad \text{(Eq. 7)}$$

$$RMSE = \sqrt{\frac{\sum_{i=1}^{n}(y_i - z_i)^2}{n}} \quad \text{(Eq. 8)}$$

where n is the number of samples, y_i represents the ground monitoring values, and z_i represents the forecast values calculated from the regression model.

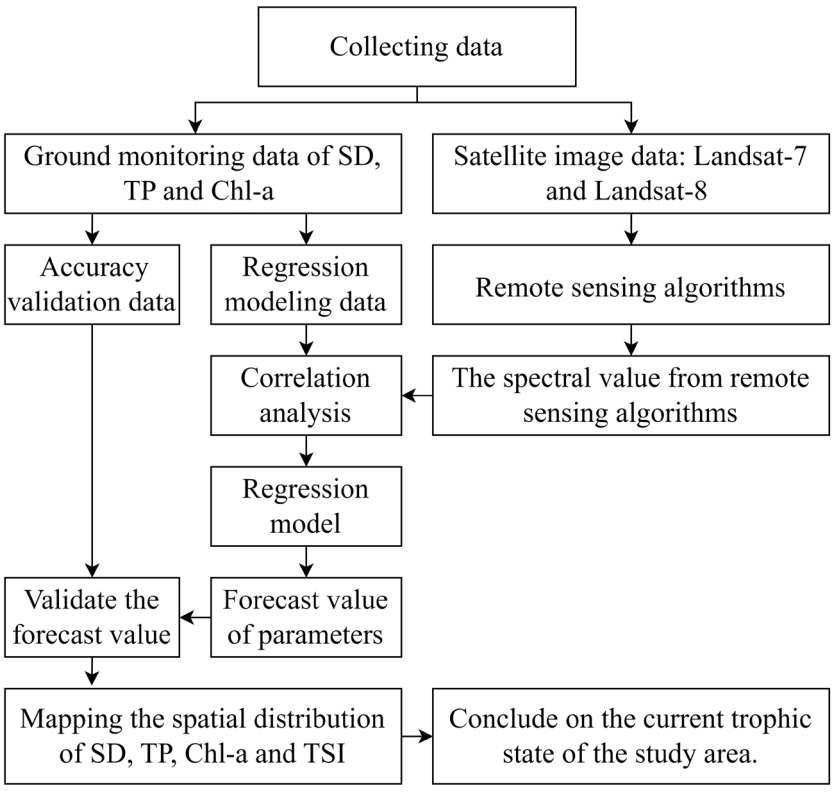

Figure 2 Methodological flowchart.

Results and discussion

1) Trophic state at ground monitoring points

The results of the analysis of the trophic state on the basis of the TSI values at the monitoring points (Figure 3) suggest that 30/35 points are eutrophic, with only 5/20 points being mesotrophic. Nevertheless, all of these mesotrophic locations have TSI values close to those of the eutrophic state. In May 2023, all 10 monitoring points had TSI values that indicated eutrophication. This shows that the water in Dau Tieng Reservoir is experiencing signs of eutrophication at most monitoring points. However, to achieve more objective conclusions about the trophic state of the reservoir, instead of conclusions based on 35 ground monitoring points, this study combines forecast value results from remote sensing methods for the entire reservoir area, as presented in the next section.

2) Spatial distribution of the trophic state

The results of the correlation analysis between the ground monitoring values and 14 remote sensing algorithms according to R (Table 4) reveal that the two parameters SD and TP correlate best with the BR3 algorithm. In contrast, the Chl-a parameter correlates best with the RVI algorithm. SD was negatively correlated, whereas TP and Chl-a were positively correlated. The p values of the ground monitoring values calculated with the BR3 and RVI algorithms for all three parameters were less than the 5% significance level, indicating that these correlations were statistically significant. The regression models of the parameters from the ground monitoring values and the spectral values from the remote sensing algorithms BR3 and RVI are presented in Figure 4. The R^2 values of the regression models are all greater than 0.8, indicating that they are robust and appropriate. Regression models can explain most of the variation in the dependent variable on the basis of changes in the independent variables. The linear equations from the regression model between the ground monitoring values and the spectral values from the remote sensing algorithms BR3 and RVI are used to calculate the forecast values for each parameter, SD, TP, and Chl-a, which correspond to Eqs. 9-11, respectively.

$$Y(SD) = -3.119X + 2.489 \quad \text{(Eq. 9)}$$

$$Y(TP) = 0.138X + 0.007 \quad \text{(Eq. 10)}$$

$$Y(Chl\text{-}a) = 54.498X - 31.171 \quad \text{(Eq. 11)}$$

In this case, Y is the forecast value, and X is the spectral value of the remote sensing algorithms.

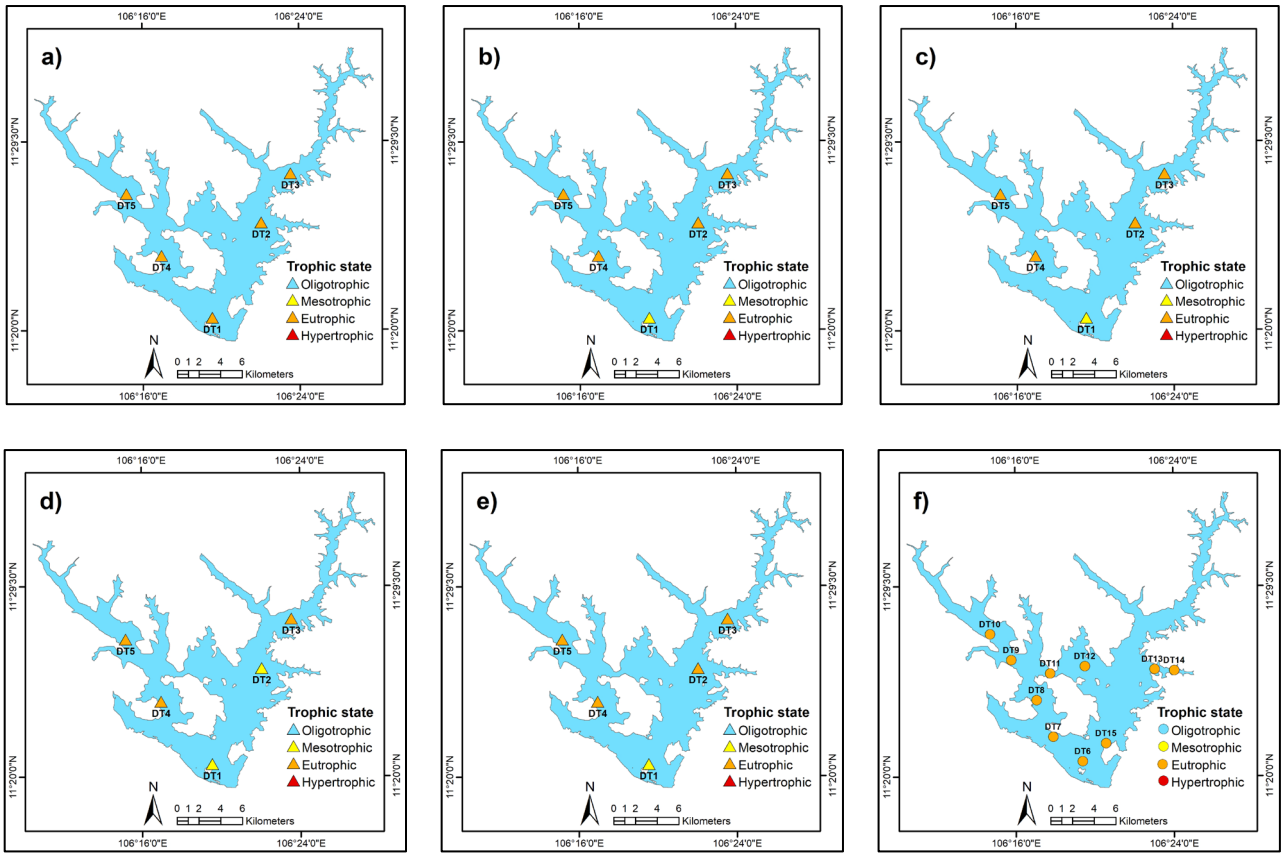

Figure 3 Trophic state at ground monitoring points: a) October 22, 2012, b) November 27, 2012, c) December 22, 2012, d) January 26, 2013, e) February 27, 2013 and f) May 6, 2023.

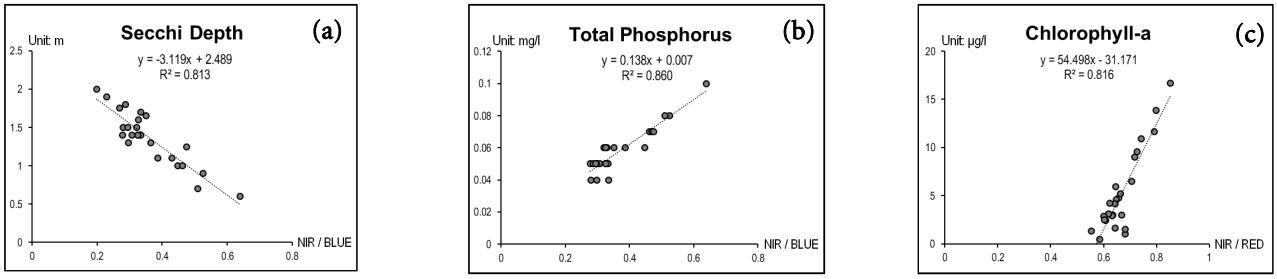

Figure 4 Regression model of parameters: (a) SD, (b) TP, and (c) Chl-a.

Table 4 Correlation analysis of ground monitoring and spectral values from remote sensing algorithms of parameters according to R

Algorithms	SD	TP	Chl-a	Algorithms	SD	TP	Chl-a
BLUE	-0.64	0.32	0.54	BR4	-0.57	0.28	0.46
GREEN	-0.61	0.33	0.56	BR5	-0.77	0.55	0.76
RED	-0.63	0.36	0.56	RVI	-0.78	0.68	**0.90**
NIR	-0.79	0.55	0.78	NDVI	-0.65	0.52	0.71
BR1	-0.46	0.26	0.51	NDWI	0.74	-0.51	-0.73
BR2	-0.59	0.32	0.55	NDTI	-0.56	0.25	0.45
BR3	**-0.81**	**0.85**	0.78	NDSSI	0.78	-0.53	-0.80

Table 5 Accuracy of the forecast values from the regression models according to the forecast errors

Parameters	MAE	MAPE	RMSE
SD (m)	0.0851	0.1531	0.0973
TP (mg L^{-1})	0.0107	0.1627	0.0129
Chl-a (µg L^{-1})	0.7155	0.0745	0.8364

The results of evaluating the accuracy of the forecast values of the parameters from the regression models according to the MAE, MAPE, and RMSE are presented in Table 5. The results show that the errors between ground monitoring and forecast values are relatively low. Therefore, regression models can be used to map the spatial distributions of parameters and trophic states according to the TSI for the entire Dau Tieng Reservoir. Spatial distribution maps of the parameters are shown in Figure 5, whereas maps of the trophic state are shown in Figure 6.

The spatial distributions of the parameters from the late rainy season to the early dry season from 2012–2013 show that at the satellite image acquisition time of October 22, 2012, the SD parameter (Figure 5a-SD) had very low values in the Northwest and Northeast Reservoir areas, whereas TP (Figure 5a-TP) and Chl-a (Figure 5a-Chl-a) had high concentrations in the entire reservoir area. A low SD indicates that the water environment has high turbidity and contains much suspended matter, whereas high concentrations of TP and Chl-an indicate that the water environment has excess nutrients. October 22, 2012, was at the end of the rainy season, the time when Dau Tieng Reservoir received water containing large amounts of nutrients from Ta On, Ta Ly, Ngo Streams, and Tha La River, leading to significantly increased turbidity and TP concentrations in the water, creating favorable conditions for algae growth. Another factor contributing to increased concentrations of nutrients in the rainy season in the Dau Tieng Reservoir is that rainwater runoff transports a large amount of fertilizer used in agricultural cultivation in alluvial areas into the aquatic environment [35]. At the satellite image acquisition times of November 27, 2012, December 22, 2012, January 26, 2013, and February 27, 2013, the TP concentrations were still high (Figures 5b to e-TP), and the SD remained low throughout the reservoir area (Figures 5b to e -SD). However, the SD values were no longer very low in the northwestern reservoir as of October 22, 2012. The Chl-a concentrations exhibited relatively significant changes at different times (Figures 5a to e-Chl-a). Specifically, from the time of the satellite images on October 22, 2012, to February 27, 2013, the Chl-a concentrations gradually decreased in the eastern and southern areas, whereas in the northeast and northwest areas of the reservoir, the Chl-a concentrations were still high. The results of the TSI calculations for all five satellite image periods from the end of the rainy season to the beginning of the dry season from 2012–2013 revealed that the trophic state of most areas of Dau Tieng Reservoir was eutrophic (Figures 6a to e), and some small areas in Northeast China and Northwestern China were hypertrophic. Only a part of the Eastern area on January 26, 2013, and February 27, 2013, was at the mesotrophic level.

In the early rainy season of May 2023, the upstream areas of the reservoir, including the North, Northwest, and Northeast Reservoir branches, all presented shallow SD values (Figure 5f-SD), whereas the TP and Chl-a concentrations were high (Figures 5f-TP & 5f-Chl-a). In addition to receiving water from tributary streams and the Tha La River, these areas are also the focus of sand mining and fish cage farming activities [20]. Sand mining activities cause increased suspended solid concentrations and water turbidity, thereby significantly reducing the amount of light transmitted, leading to low SD values in these areas. For cage fish farming activities, the amount of leftover food and waste from the farming process is the leading cause of increased TP concentrations in water, promoting phytoplankton growth. The SD values and TP and Chl-a concentrations in the Dau Tieng Reservoir water source are strongly influenced by season, hydro-logical regime, and human activities. The results of calculating the TSI value at satellite image acquisition times of May 6, 2023, show that eutrophication is severe in most Dau Tieng Reservoir areas (Figure 6f), except for a small part of the Eastern Reservoir. In particular, the upstream area of the reservoir is in a hypertrophic state.

When aquatic environments contain nutrients, these nutrients are gradually removed through microbial decomposition, which plays a crucial role in the carbon cycle. Initially, aerobic microorganisms in the surface layer utilize dissolved oxygen to decompose organic matter. These processes transfer organic carbon into inorganic forms of carbon, primarily carbon dioxide (CO_2), which is released into the atmosphere or taken up by aquatic plants for photosynthesis. However, when eutrophication occurs, these processes significantly deplete dissolved oxygen, depriving aquatic organisms of the oxygen required for respiration and triggering a cascade of ecological effects [36]. As excessive organic matter accumulates and cannot be fully decomposed at the surface layer, the remaining debris sinks to the bottom. In this oxygen-deficient environment, anaerobic microorganisms decompose the material, producing methane (CH_4) and hydrogen sulfide (H_2S). Methane, a potent greenhouse gas, becomes a part of the global carbon cycle when released into the atmosphere. These processes degrade habitats by introducing toxic compounds and creating hypoxic or anoxic zones, making survival difficult for many aquatic organisms. Sensitive species may die off or migrate, reducing biodiversity and disrupting the balance of the ecosystem [37].

Furthermore, algal blooms, fueled by nutrient pollution, are among the most common consequences of such imbalances [38]. Some species of algae, such as blue–green algae, produce toxins that can accumulate in living organisms and spread along the food chain from zooplankton to small fish, large fish, and even humans, potentially causing poisoning or death. When algae bloom, the dense growth of algal cells covers the water surface, preventing oxygen from diffusing from the air into the water. Additionally, the respiratory activity of algae at night, especially when the algae density is high, further depletes dissolved oxygen in the water. Although algal blooms temporarily sequester carbon by increasing its biomass during photosynthesis, this carbon is quickly returned to the environment when the algae die and decompose. As algae die, their decomposition consumes a substantial amount of dissolved oxygen, leading to the formation of 'dead zones' where oxygen is completely depleted. These zones make aquatic habitats uninhabitable and disrupt the carbon cycle. The decomposition of algal biomass releases large amounts of carbon dioxide. Moreover, anaerobic conditions in the bottom layers contribute to methane production, exacerbating climate change and further disturbing the ecological balance of aquatic systems [36].

The Dau Tieng Reservoir is an important water source for the daily needs and production activities of residents and neighboring areas. Recent studies have also indicated that reservoirs are experiencing algal blooms [20] and a decline in water quality [35]. Therefore, monitoring, minimizing pollution and ensuring water security are incredibly urgent. The approach in this study shows that remote sensing methods can be applied to monitor and assess the trophic state of reservoirs. Compared with the results of the trophic state assessment at monitoring points and the estimated results from satellite image data, 34/35 points are similar. The validation results from the forecast errors also show that the deviation is relatively low. The advantage of the remote sensing method is that it can provide detailed data and information in real time on the basis of continuously updated satellite image data, helping to save costs and time and allowing proactive management and intervention. However, the disadvantage of this method is that it needs to be combined with ground measurement data to be able to construct an accurate and reliable forecast model. The limited number of ground monitoring points is a drawback in this study. In addition, during the rainy season, satellite image data are often affected by weather conditions, so the support of traditional measurement methods is still needed for continuous monitoring.

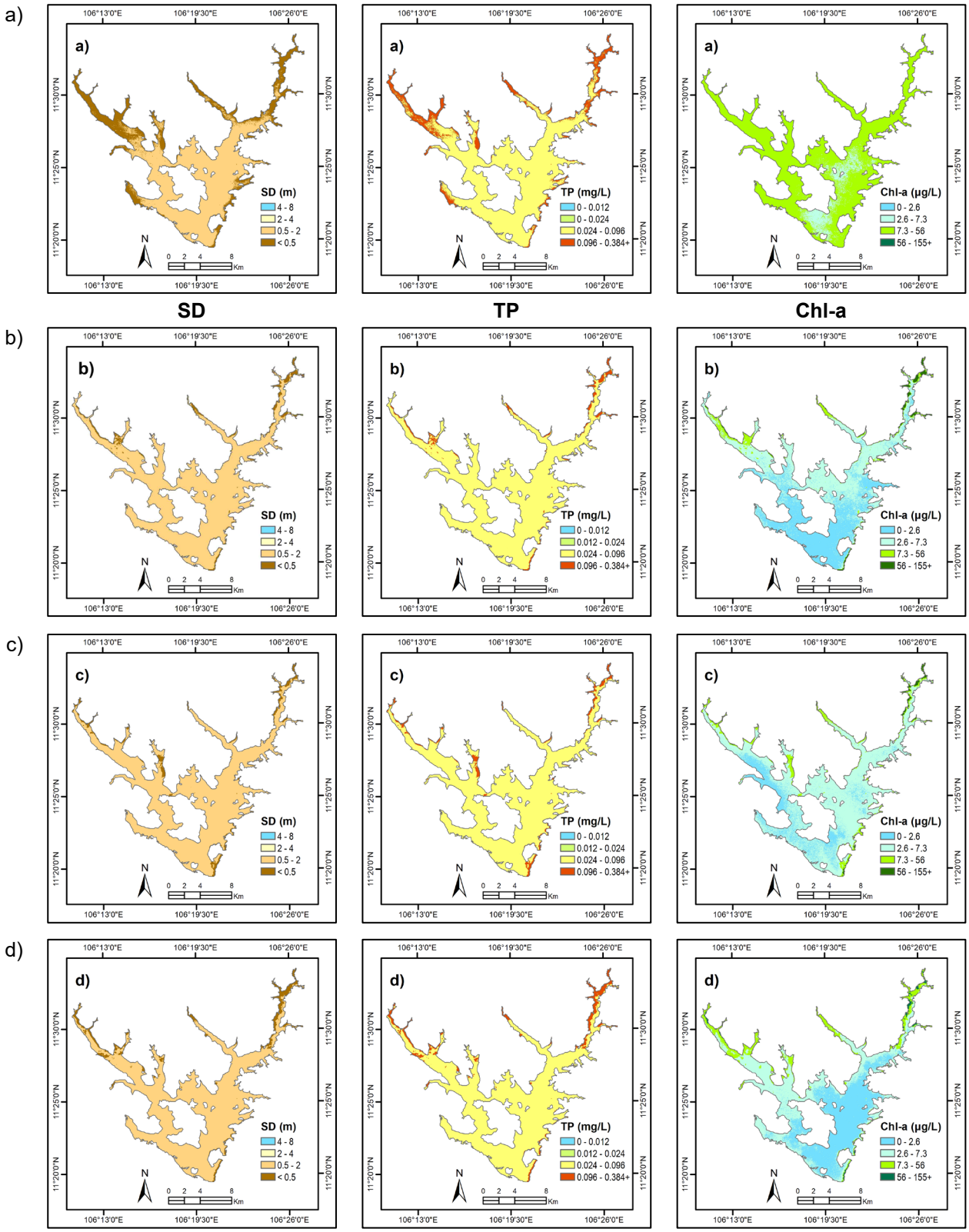

Figure 5 SD, TP, and Chl-a spatial distributions at satellite image acquisition times: a) October 22, 2012, b) November 27, 2012, c) December 22, 2012, d) January 26, 2013, e) February 27, 2013, and f) May 6, 2023

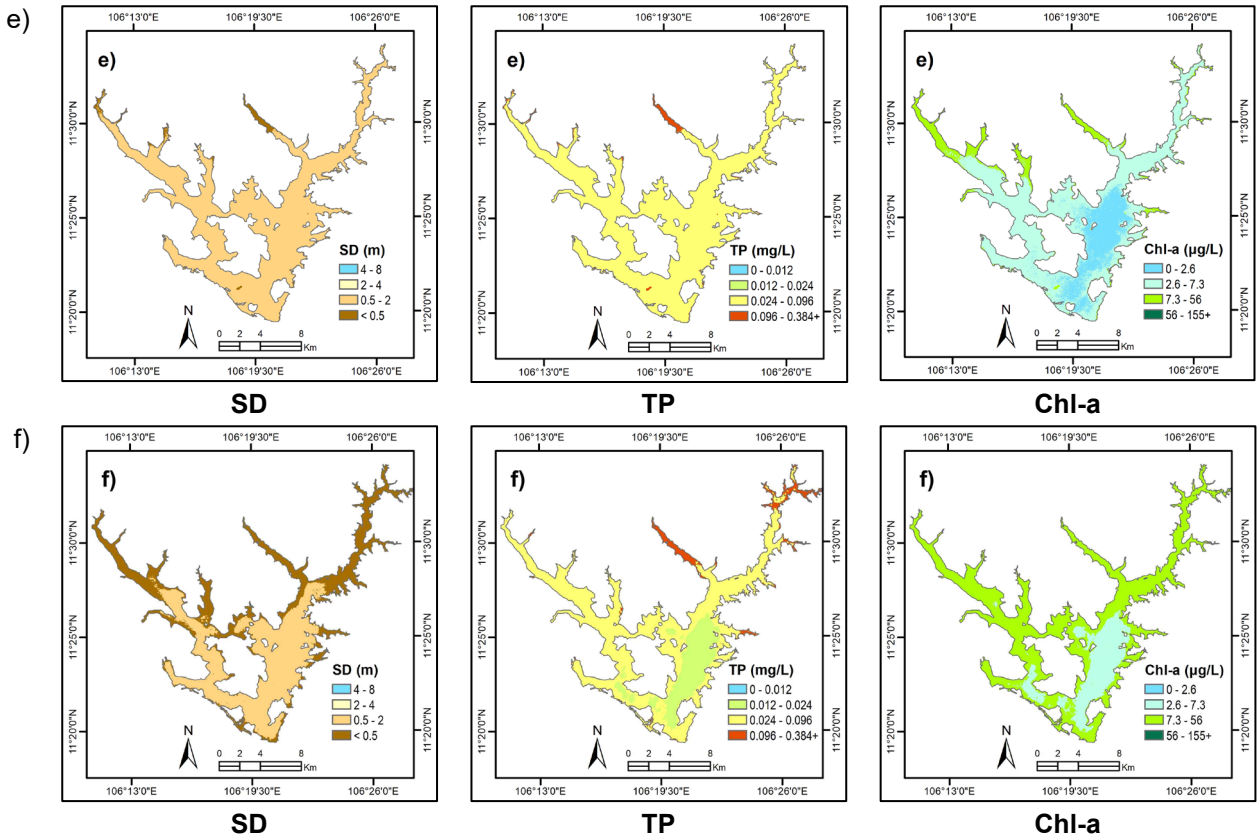

Figure 5 SD, TP, and Chl-a spatial distributions at satellite image acquisition times: a) October 22, 2012, b) November 27, 2012, c) December 22, 2012, d) January 26, 2013, e) February 27, 2013, and f) May 6, 2023 *(continued)*.

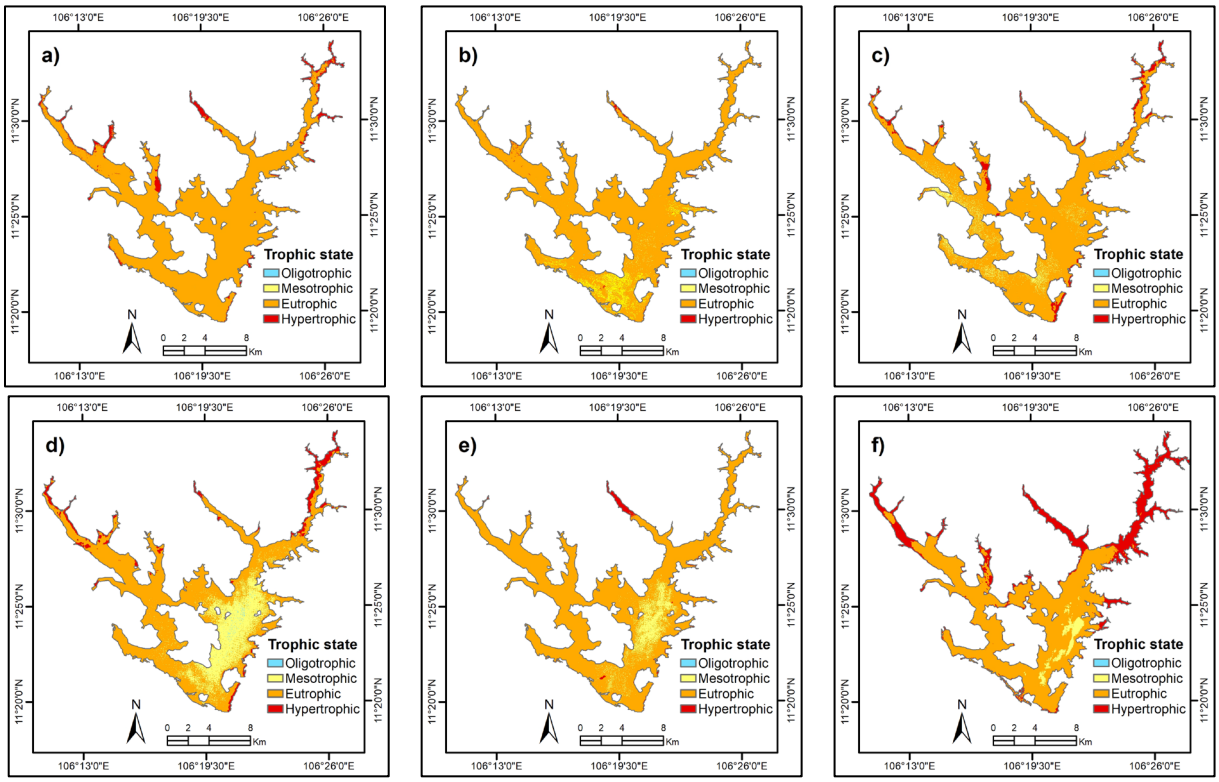

Figure 6 Spatial estimation of the trophic state at satellite image acquisition times: a) October 22, 2012, b) November 27, 2012, c) December 22, 2012, d) January 26, 2013, e) February 27, 2013, and f) May 6, 2023.

Conclusions

This study presents a technique for mapping trophic states according to Carlson's TSI via remote sensing methods for the Dau Tieng Reservoir. The dataset from the late rainy season to the early dry season from 2012–2013 estimate the forecast values of the SD, TP, and Chl-a parameters in the early rainy season of May 2023. The spatial distribution results of the TSI value show that in the Dau Tieng Reservoir area on May 6, 2023, eutrophication occurred in most reservoir areas and, in some places, was even hypertrophic. Despite some limitations in input data, such as the number of samples used in the regression model and the assessment of the accuracy of forecast value results being quite limited, research has demonstrated the feasibility of applying remote sensing methods in assessing the trophic state of the Dau Tieng Reservoir. The spectral reflectance characteristics of monitoring objects are factors that increase the possibility and accuracy of research. This study will be a source of consultation and a stepping stone to developing remote sensing algorithms for further research to monitor nutrient status and water quality in water bodies. The study results also warn relevant parties about the current state of nutrient pollution in the Dau Tieng Reservoir. It is necessary to have synchronous and timely solutions in reservoir water environmental management to reduce pollution, improve water quality, and protect the ecosystem in the area. Our next research direction will be to increase the number of ground monitoring samples used in the correlation analysis, build regression models, and validate the results from the models. This allows us to build a rigorous regression model with high accuracy that can be applied in practice to monitor the trophic state of water bodies.

Acknowledgments

We would like to thank Ho Chi Minh City University of Technology (HCMUT), VNU-HCM, for the support of time and facilities for this study. The authors are grateful to the United States Geological Survey (USGS) and the National Aeronautics and Space Administration (NASA) for accessing the satellite imagery used for this study.

References

[1] Walters, A. Nutrient pollution from agricultural production: Overview,
management and a study of Chesapeake Bay. New York: Nova Science Publishers, 2016.

[2] Chapin, F.S., Matson, P.A., Vitousek, P.M. Principles of terrestrial ecosystem ecology. 2nd Edition. New York: Springer, 2011.

[3] Watson, S.B., Whitton, B.A., Higgins, S.N., Paerl, H.W., Brooks, B.W., Wehr, J.D. Harmful algal blooms. *In:* Wehr, J.D., Sheath, R.G., Kociolek, J.P. (2nd Edition), Freshwater algae of North America. California: Academic Press, 2015, 873–920.

[4] Trung, B., Dao, T.S., Faassen, E., Lürling, M. Cyanobacterial blooms and microcystins in Southern Vietnam. Toxins, 2018, 10(11), 471.

[5] Augusto-Silva, P.B., Ogashawara, I., Barbosa, C.C.F., De Carvalho, L.A.S., Jorge, D.S.F., Fornari, C.I., Stech, J.L. Analysis of MERIS reflectance algorithms for estimating chlorophyll-a concentration in a Brazilian Reservoir. Remote Sensing, 2014, 6, 11689–11707.

[6] Johansen, R., Beck, R., Nowosad, J., Nietch, C., Xu, M., Shu, S., …, Su, H. Evaluating the portability of satellite derived chlorophyll-a algorithms for temperate inland lakes using air-borne hyperspectral imagery and dense surface observations. Harmful Algae, 2018, 76, 35–46.

[7] Buma, W.G., Lee, S.-I. Evaluation of Sentinel-2 and Landsat 8 Images for Estimating Chlorophyll-a Concentrations in Lake Chad, Africa. Remote Sensing, 2020, 12(5), 2437.

[8] Duan, H., Zhang, Y., Zhang, B., Song, K., Wang, Z. Assessment of chlorophyll-a concentration and trophic state for Lake Chagan using landsat TM and field spectral data. Environmental Monitoring and Assessment, 2007, 129, 295–308.

[9] Papoutsa, C., Akylas, E., Hadjimitsis, D. Trophic State Index derivation through the remote sensing of Case-2 water bodies in the Mediterranean region. Central European Journal of Geosciences, 2014, 6(1), 67–78.

[10] Membrillo-Abad, A.S., Torres-Vera, M.A., Alcocer, J., Prol-Ledesma, R.M., Oseguera, L.A., Ruiz-Armenta, J.R. Trophic state index estimation from remote sensing of lake Chapala, Mexico. Revista Mexicana de Ciencias Geológicas, 2016, 33(2), 183–191.

[11] Shi, K., Zhang, Y., Song, K., Liu, M., Zhou, Y., Zhang, Y., …, Qin, B. A semi-analytical approach for remote sensing of trophic state in inland waters: Bio-optical mechanism and application. Remote Sensing of Environment, 2019, 232, 111349.

[12] Carlson, R.E. A trophic state index for lakes. Limnology and Oceanography, 1977, 22(2), 361–369.

[13] Lyu, L., Song, K., Wen, Z., Liu, G., Shang, Y., Li, S., …, Hou, J. Estimation of the lake trophic state index (TSI) using hyperspectral remote sensing in Northeast China. Optics Express, 2022, 30(7), 10329–10345.

[14] Nguyen, H.T.T., Vu, H.T., Nguyen, N.T.P., Doan, K.M.T. Monitoring the trophic state index of Linh

Dam Lake using Landsat 8 Imagery. Journal of Mining and Earth Sciences, 2017, 58(3), 42–50.

[15] Tuan, D.H., Mung, V.T., Cuong, D.M. Evaluation of water quality of a blue lake at An Son Commune, Thuy Nguyen District, Hai Phong City by water quality index (WQI), trophic state index (TSI) and heavy metal pollution index (HPI). VNU Science Journal: Earth and Environmental Sciences, 2017, 33(1), 45–54.

[16] Ngoc, N.T.B., An, V.D., Quynh, L.T.P., Thuy, N.T.B., Nghia, L.D., Thuy, D.T., Cuong, H.T. Assessment of the trophic status in some lakes within Hanoi inner city. Vietnam Journal of Science and Technology, 2017, 55(1), 84–92.

[17] Thuan, T.D., Lap, B.Q., Thanh, L.M., Harada, M. Eutrophication Status of Lakes in Inner Hanoi and a Cu Chinh Lake Case Study. Journal of the Faculty of Agriculture Kyushu University, 2021, 66(1), 97–104.

[18] Carlson, R.E., Simpson, J. A coordinator's guide to volunteer lake monitoring methods. North American Lake Management Society, 1996.

[19] Thao, N.T.P, Vinh, P.Q., Ha, N.T.T., Linh, N.T. Monitoring the eutrophication level of Lake Hoan Kiem based on the estimated Chlorophyll–a concentration from Sentinel-2A imagery. Journal of hydro-meteorology, 2021, 721, 11–20.

[20] Thong, N.H., Van, T.T., Dao, T.S. Mapping of the algae distribution to support water quality management in the Dau Tieng reservoir. Carpathian Journal of Earth and Environmental Sciences, 2023, 18(2), 415–427.

[21] Pham, T.L., Dao, T.S., Tran, N.D., Nimptsch, J., Wiegand, C., Motoo, U. Influence of environmental factors on cyanobacterial biomass and microcystin concentration in the Dau Tieng Reservoir, a tropical eutrophic water body in Vietnam. Annales de Limnologie - International Journal of Limnology, 2017, 53, 89–100.

[22] American Public Health Association. APHA method 4500-P: Standard methods for the examination of water and wastewater. Washington, D.C.: American Public Health Association, 2012.

[23] American Public Health Association. APHA method 10200-PLANKTON: Standard methods for the examination of water and wastewater. Washington, D.C.: American Public Health Association, 2012.

[24] Gitelson, A. The peak near 700 nm on radiance spectra of algae and water: relationships of its magnitude and position with chlorophyll concentration. International Journal of Remote Sensing, 1992, 13(17), 3367–3373.

[25] Richardson, L.L. Remote sensing of algal bloom dynamics. BioScience, 1996, 46(7), 492–501.

[26] Olli V., Emanuela C., Esa T. Chlorophyll does not reflect green light – how to correct a misconception. Journal of Biological Education, 2020, 56(5), 1–8.

[27] Du, C., Wang, Q., Li, Y., Lyu, H., Zhu, L., Zheng, Z., …, Guo, Y. Estimation of total phosphorus concentration using a water classification method in inland water. International Journal of Applied Earth Observation and Geoinformation, 2018, 71, 29–42.

[28] Ren, W., Wu, X., Chen, B., Chao, J., Ge, X., Yan, J., Yang, H. Optical characteristics of chromophoric dissolved organic matter (CDOM) in upstream and downstream lakes of Taihu Lake Basin: New insights for water environmental management. Chinese Geographical Science, 2022, 32(4), 606–619.

[29] Coble, P.G. Marine Optical biogeochemistry: The chemistry of ocean color. Chemical Reviews, 2007, 107(2), 402–418.

[30] Jordan, C.F. Derivation of leaf-area index from quality of light on the forest floor. Ecology, 1969, 50(4), 663–666.

[31] Rouse, J.W., Haas, R.H., Schell, J.A., Deering, D.W. Monitoring vegetation systems in the Great Plains with ERTS. In Proceedings of the Third ERTS-1 Symposium NASA, Washington, D.C., 10-12 December 1974, 309–317.

[32] McFeeters, S.K. The use of the normalized difference water index (NDWI) in the delineation of open water features. International Journal of Remote Sensing, 1996, 17(7), 1425–1432.

[33] Lacaux, J.P., Tourre, Y.M., Vignolles, C., Ndione, J.A., Lafaye, M. Classification of ponds from high-spatial resolution remote sensing: Application to Rift Valley Fever epidemics in Senegal. Remote Sensing of Environment, 2007, 106(1), 66–74.

[34] Hossain, A.K.M., Yafei, J., Xiaobo, C. Development of remote sensing based index for estimating/ mapping suspended sediment concentration in river and lake environments. In Proceedings of the 8th International Symposium on Ecohydraulics (ISE 2010), Zaragoza, Spain, 12–16 September 2010, No. 0435, 578–585.

[35] Van, T.T., Bao, H.D.X., My, N.T., Thong, N.H., Phuong, D.T.K., Truong, N.T., …, Trinh, H.B.V. Assessment of Dau Tieng reservoir water quality using standard criteria combined with remotely sensed images. Geodetski vestnik, 2023, 67(3), 343–362.

[36] Carpenter, S.R., Caraco, N.F., Orrell, D.L., Howarth, R.W., Sharpley, A.N., Smith, V.H. Nonpoint pollution of surface waters with phosphorus and nitrogen. Ecological Applications, 1998, 8(3), 559–568.

[37] Horne, A.J., Goldman, C.R. Limnology. USA: McGraw-Hill, 1994, 576.
[38] Smith, V.H., Joye, S.B., Howarth, R.W. Eutrophication of freshwater and marine ecosystems. Limnology and Oceanography, 2006, 51(1), 351–355.